Radiative decays of the J/ψ into $\gamma\pi^+\pi^-$ and γK^+K^-

R. M. Baltrusaitis, D. Coffman, G. Dubois, G. Eigen, J. Hauser, D. G. Hitlin, C. G. Matthews, J. D. Richman, J. J. Russell, and Y. Zhu
California Institute of Technology, Pasadena, California 91125

T. Bolton, K. O. Bunnell, R. E. Cassell, D. H. Coward, S. Dado, D. Favart, K. F. Einsweiler, U. Mallik, R. F. Mozley, A. Odian, J. Roehrig, R. H. Schindler, W. Stockhausen, W. Toki, F. Villa, S. Wasserbaech, N. Wermes, D. E. Wisinski, and G. Wolf
Stanford Linear Accelerator Center, Stanford, California 94305

D. E. Dorfan, R. Fabrizio, F. Grancagnolo, R. P. Hamilton, C. A. Heusch, L. Köpke, W. S. Lockman, R. Partridge, J. Perrier, H. F. W. Sadrozinski, M. Scarlatella, T. L. Schalk, A. Seiden, A. J. Weinstein, and R. Xu
University of California at Santa Cruz, Santa Cruz, California 95064

J. J. Becker, G. T. Blaylock, B. I. Eisenstein, T. Freese, G. Gladding, S. A. Plaetzer, C. Simopoulos, A. L. Spadafora, I. E. Stockdale, J. J. Thaler, B. Tripsas, A. Wattenberg, and W. J. Wisniewski
University of Illinois, Champaign-Urbana, Illinois 61801

J. S. Brown, T. H. Burnett, V. Cook, A. L. Duncan, A. D. Guy, P. M. Mockett, A. Nappi, B. Nemati, J. C. Sleeman, and H. J. Willutzki
University of Washington, Seattle, Washington 98195
Mark III Collaboration

(Received 14 October 1986)

The decays $J/\psi\to\gamma\pi^+\pi^-$ and $J/\psi\to\gamma K^+K^-$, $M_{K^+K^-}<2.0$ GeV/c^2, have been studied. Measurements are presented for $B(\psi\to\gamma f(1270))B(f(1270)\to\pi^+\pi^-)$, $B(\psi\to\gamma\theta(1720))B(\theta(1720)\to\pi^+\pi^-)$, $B(\psi\to\gamma f'(1525))B(f'(1525)\to K^+K^-)$, and $B(\psi\to\gamma\theta)B(\theta(1720)\to K^+K^-)$. A higher-mass structure is observed in the $\pi^+\pi^-$ channel. The spin of the $\theta(1720)$ is established with high confidence. The polarization structure of the $f(1270)$, $f'(1525)$, and $\theta(1720)$ have been determined.

I. INTRODUCTION

This paper deals with J/ψ radiative decays to $\pi^+\pi^-$ systems of all kinematically accessible invariant masses and to K^+K^- systems below 2.0 GeV/c^2 (Ref. 1). $K\bar{K}$ masses above 2.0 GeV/c^2 have been treated separately.[2]

Quantum chromodynamics (QCD) admits the possibility of colorless bound states of two or more gluons, which have been named glueballs. Radiative decays of the J/ψ have been suggested[3] as promising modes for glueball searchs. The ratio of J/ψ decays via γgg to those via ggg, according to perturbative QCD, is

$$\frac{\Gamma(J/\psi\to\gamma gg)}{\Gamma(J/\psi\to ggg)}=\frac{36}{5}e_q^{\,2}\frac{\alpha}{\alpha_s}\left[1+\frac{2.2\alpha_s}{\pi}+\cdots\right]^2.$$

For $\alpha_s=0.2$, this leads to a branching fraction $B(J/\psi\to\gamma 2g)\sim 5-10\,\%$. Thus, a substantial fraction of all J/ψ decays are expected to proceed through the radiative decay diagram. Hadronic final states produced from the two-gluon system have $C=+$ and $I=0$.

It was calculated[4] that $J^{PC}=0^{++},0^{-+},2^{++}$ dominate the $J/\psi\to\gamma X$ final state and that $J^{PC}=1^{--}$ and 1^{-+} are suppressed. The final states most accessible are those containing two or three pseudoscalars. Two pseudoscalars can combine to produce states with $J^{PC}=0^{++},2^{++}$ while three pseudoscalars can form $J^{PC}=0^{-+}$ states.

In the 2^{++} channel, the $f(1270)$ appears very prominently in the $\pi\pi$ mode. The production characteristics (i.e., the population of the different polarization states) of this final state have been measured by the Mark II and Crystal Ball experiments.[5,6] The $f'(1525)$ has been seen by the Mark II experiment[7] in the K^+K^- final state. The $\theta(1720)$ has been observed in the $\eta\eta$ and K^+K^- decay modes by the Crystal Ball and Mark II experiments, respectively; they have only set limits on its decay to $\pi\pi$ (Refs. 7 and 8). The $\theta(1720)$ has been suggested as a glueball candidate.[9] The $S^*(975)$, an $I=0$, 0^{++} state, is notably absent from radiative J/ψ decays.

II. THE MARK III DETECTOR

The Mark III detector[10] is a general-purpose magnetic spectrometer, optimized for the SPEAR energy region. The design goal was a detector capable of complete reconstruction of exclusive final states. At the SLAC storage ring SPEAR, the mean charged and neutral multiplicities are each about four. The momentum spectra for charged and neutral particles peaks at 500 and 250 MeV/c, respectively. The salient features of the detector are (1) a beryllium beam pipe with a low-mass trigger chamber to minimize multiple scattering, (2) a charged-track solid-angle coverage of 85% of 4π, and a neutral track coverage of 95% of 4π, (3) good particle identification for the charged tracks using a time-of-flight (TOF) system with a resolution of 190 ps, (4) a finely segmented shower counter with good detection efficiency for low-energy photons, good electron-hadron separation, and an energy resolution of $\Delta E/E=17\%/\sqrt{E}$, and (5) two layers of steel and muon counters outside the solenoidal coil for muon-hadron separation covering 65% of 4π. The detector design is shown in axial and transverse views in Figs. 1 and 2, respectively.

III. THE $\gamma\pi^+\pi^-$ FINAL STATE

Event selection for $J/\psi\rightarrow\gamma\pi^+\pi^-$

The radiative photon must be observed in the shower counter. Events are required to have fewer than five isolated photons, where "isolated" means $\cos\theta_{\gamma\pi}<0.95$. More than one photon is allowed since the products of charged hadrons interacting in the shower counter are sometimes counted as photons.

The number of kaons produced in J/ψ decays is much smaller than the number of pions, so that no particle identification by TOF is required for π's. This results in a higher efficiency due to greater solid-angle coverage. The kaons in the sample are removed later by kinematic fitting.

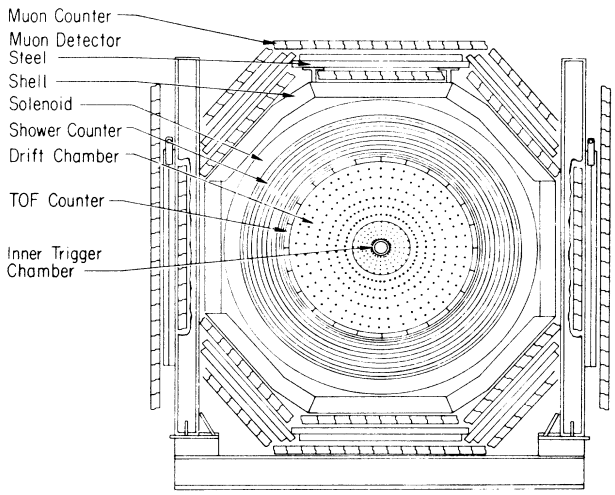

FIG. 1. The axial view of the Mark III detector.

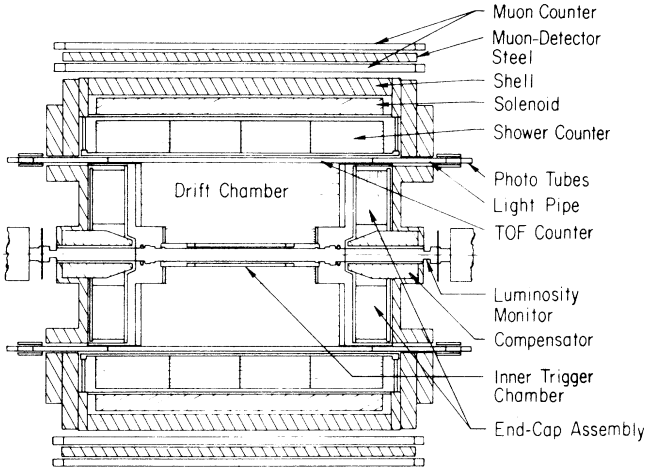

FIG. 2. The transverse view of the Mark III detector.

The muon system is used to reject $\gamma\mu^+\mu^-$ events. To avoid biases due to hadronic punch-through, events are rejected only if one track is detected in both layers in the muon system and the other track is found in at least one muon layer.

The $\gamma\pi^+\pi^-$ candidates are preselected for fitting using simple kinematic cuts. Two variables are used: a "missing-neutral-energy" variable U (Ref. 11) and a "missing-p_t" variable $p_{t_\gamma}{}^2$ (Ref. 11). The U variable is defined as $U=E_{\rm miss}-|P_{\rm miss}|$, where $E_{\rm miss}$ and $P_{\rm miss}$ are the missing energy and momentum, calculated from the charged-track momenta by using the pion mass hypothesis. The resolution is U is approximately independent of the missing momentum. A cut to include events with $|U|<0.2$ GeV is made, corresponding to $\sim 3\sigma$ in the resolution. The sample remaining after such a cut is dominated by the $\pi^+\pi^-\pi^0$ and the $\gamma\pi^+\pi^-$ final states.

The $p_{t_\gamma}{}^2$ variable is defined by the relation

$$p_{t_\gamma}{}^2=4P_{\rm miss}{}^2\sin^2\frac{\theta}{2}\ ,$$

where θ is the angle between $P_{\rm miss}$ and the direction of the photon. This variable measures the agreement between the missing momentum recoiling against the charged tracks and the angles of the photon in the event. It uses the fact that the angles and magnitude of the missing momentum are well measured by the drift chamber, whereas only the angles of the photon are well measured by the shower counter. The background from $\pi^+\pi^-\pi^0$ is approximately flat in this variable for values up to $p_{t_\gamma}{}^2\sim m_{\pi^0}{}^2$, whereas the radiative signal is peaked at small values $p_{t_\gamma}{}^2\simeq 0.001$ (GeV/c)^2. The distribution in $p_{t_\gamma}{}^2$ for the candidate $\gamma\pi^+\pi^-$ events which have passed the U cut is shown in Fig. 3(a). Signal events are required to have $p_{t_\gamma}{}^2<0.002$; this cut suppresses more than 80% of the $\pi^+\pi^-\pi^0$ background.

To improve the mass resolution and increase the ability to reject background, four-constraint fits are done by imposing energy and momentum conservation. The ability

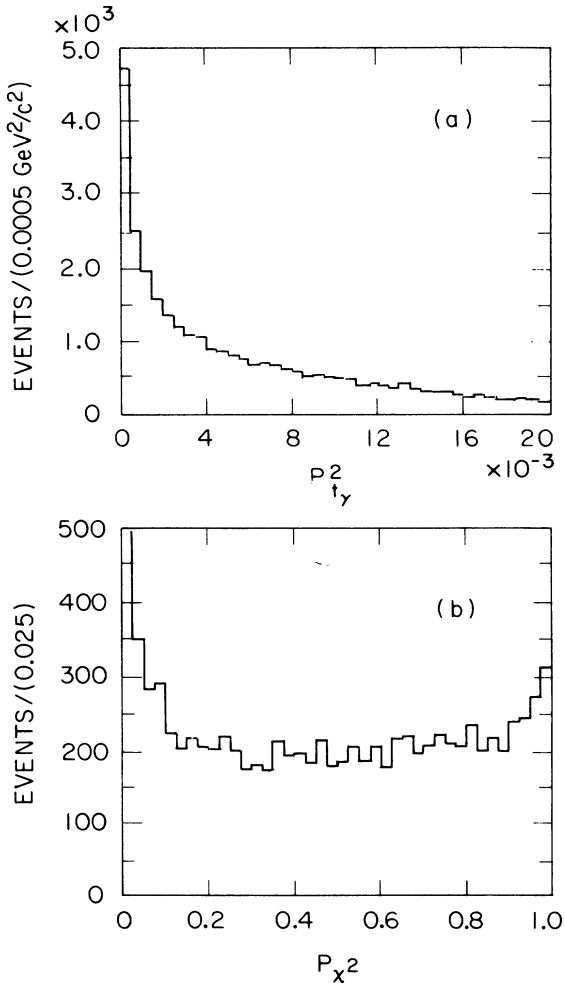

FIG. 3. Kinematic variables for $J/\psi\to\gamma\pi^+\pi^-$. (a) The $p_{t_\gamma}{}^2$ distribution for events which have passed a loose U cut. (b) The kinematic-fit confidence level, P_{χ^2}, after a $P_{t_\gamma}{}^2$ cut.

of the kinematic fit to discriminate between signal and background is important in this analysis, as it partially makes up for insufficient TOF information.

Fits are performed using all permutations of the photon candidates in the event. Two parallel hypotheses are examined, representing the signal of interest ($J/\psi\to\gamma\pi^+\pi^-$) as well as the largest background ($J/\psi\to\gamma\gamma\pi^+\pi^-$). For the events passing the $P_{t_\gamma}{}^2$ cut, the P_{χ^2} distribution for the $\gamma\pi\pi$ hypothesis is shown in Fig. 3(b). The combination with the best fit to $\gamma\pi^+\pi^-$ is retained if the confidence level is ≥ 0.05. A Monte Carlo simulation shows that with this cut there is little kaon contamination, even without the particle identification from the time-of-flight counters.

The $\pi^+\pi^-$ mass distribution resulting from these kinematic cuts is shown in Fig. 4. There is evidence for a $\rho^0(770)$ peak due to feed-through from the $J/\psi\to\rho^0\pi^0$ channel, an $f(1270)$ peak due to real radiative events, and a large background from $J/\psi\to\rho^\pm\pi^\mp$.

The background coming from $J/\psi\to\pi^0\pi^+\pi^-$ originates in events in which the π^0 decays asymmetrically and one photon is lost. This configuration is kinematically indistinguishable, for finite resolution, from the desired single-photon topology, since the low-energy photon carries away a negligible momentum. Thus, despite the cuts that have been applied, $J/\psi\to\pi^+\pi^-\pi^0$ remains the dominant source of background in this final state. Figure 5(a) shows the mass distribution for $J/\psi\to\pi^+\pi^-\pi^0$ events which have been kinematically fit to the $J/\psi\to\gamma\gamma\pi^+\pi^-$ hypothesis, with an additional requirement: $0.08\leq m_{\gamma\gamma}\leq 0.19$ GeV/c^2. The ρ^0 mass peak is visible, and the broader peak at higher mass is the kinematic reflection of the $\rho^\pm\pi^\mp$ events. The Dalitz plot shows the dominance of the two-body $\rho\pi$ final state, which is confined to a small region of the total phase space, as seen in Fig. 5(b).

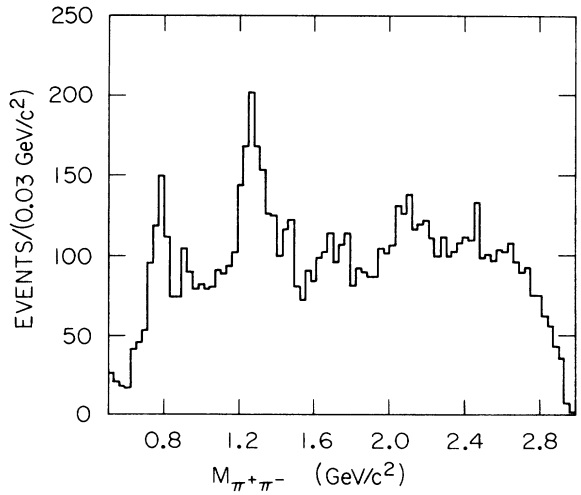

FIG. 4. The $\pi^+\pi^-$ mass distribution after kinematic cuts.

If additional electron-hadron identification is employed to reject electrons, using information from the shower counter, the mass distribution changes as shown in Fig. 6(a), and the corresponding Dalitz plot is shown in Fig. 6(b). States with a fixed $\pi^+\pi^-$ mass appear as diagonal bands. The $\rho^\pm\pi^\mp$ background is visible in the Dalitz plot in the form of bands at the edges of the plot. Events lying outside the $\rho\pi$ bands correspond to real $\gamma\pi^+\pi^-$ decays, as they cannot be attributed to other background processes.

Two fits are performed to determine the mass and width of the $f(1270)$. One has the width fixed at 0.180 GeV/c^2, the value quoted by the Particle Data Group,[12] while the other allows the width to vary. The results are shown in Fig. 7, where a simple polynomial has been used to represent the background. The results of these fits are

$$m=1.269^{+0.013}_{-0.013}\ \text{GeV}/c^2,\quad \Gamma\equiv 0.180\ \text{GeV}/c^2\ \text{(fixed)}$$

and

$$m=1.268^{+0.012}_{-0.012}\ \text{GeV}/c^2,\quad \Gamma=0.139^{+0.055}_{-0.039}\ \text{GeV}/c^2,$$

where the quoted errors represent the statistical uncertainty of the fit. The fits are consistent, but the narrower width corresponds to a smaller number of events in the

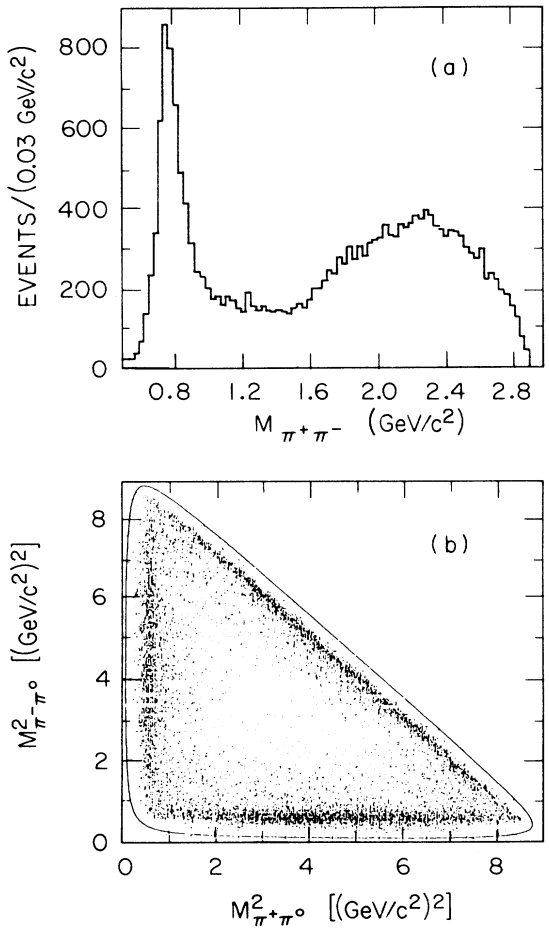

FIG. 5. (a) The $\pi^+\pi^-$ mass spectrum and (b) the Dalitz plot for $J/\psi\to\rho\pi$.

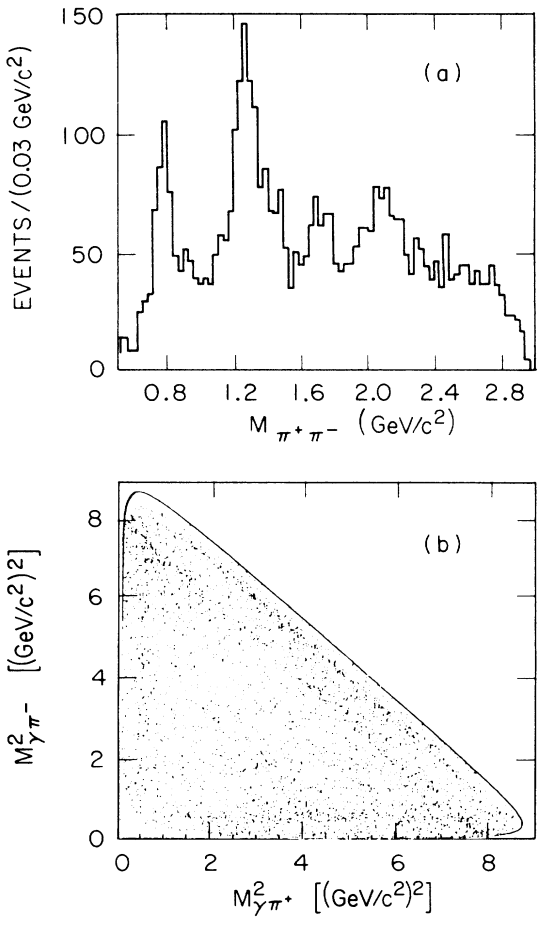

FIG. 6. (a) The $\pi^+\pi^-$ mass distribution after additional electron cuts and (b) the Dalitz plot.

peak. In extracting the branching ratio for the $f(1270)$, the width is fixed at 0.180 GeV/c^2.

The detection efficiency is calculated by generating and reconstructing Monte Carlo events with the correct mass, width, and angular distributions for the $f(1270)$. The actual parameters used for the Monte Carlo generation were

$$m=1.270\ \text{GeV}/c^2,\quad \Gamma=0.180\ \text{GeV}/c^2\ ,$$

$$x=0.88,\quad y=0.04,\quad \varphi_x=\varphi_y=0\ ,$$

where the helicity-amplitude ratios x and y are defined in the next section. The values are taken from the measurement of the Crystal Ball Collaboration for the $\gamma\pi^0\pi^0$ final state,[6] rather than from the current analysis, since the $\gamma\pi^0\pi^0$ state does not suffer from the hadronic ($\rho\pi$) background problems inherent in the charged state. The efficiency is found to be 0.38 ± 0.05. Using this efficiency, the branching ratio is

$$B(J/\psi\to\gamma f(1270))B(f(1270)\to\pi^+\pi^-)$$
$$=(7.66\pm0.5\pm1.3)\times10^{-4}\ ,$$

where the systematic error includes the uncertainties from the Monte Carlo efficiency calculation, the form of the angular distribution, the number of produced J/ψ events, and the value of the width in the fit.

Spin analysis of the $f(1270)$ region

The spin analysis of X in the decay sequence $J/\psi\to\gamma X$, $X\to0^-0^-$ is performed by studying the angular distributions of the radiated photon and one of the two pseudoscalars. A boson-antiboson pair produced in radiative J/ψ decays must have $J^{PC}=(\text{even})^{++}$. For the $J=0$ case, the angular distributions are completely predicted. For $J\geq2$, the angular distributions depend on several, *a priori* unknown, parameters, which in the helicity formalism,[13] describe the relative populations of the allowed polarization states of X. Parity invariance reduces the number of complex helicity parameters from seven to three, denoted by A_0, A_1, and A_2. By taking ratios, these six real quantities are further reduced to four, defined as

$$xe^{i\phi_x}\equiv\frac{A_1}{A_0},\quad ye^{i\phi_y}=\frac{A_2}{A_0}\ ;$$

x and y are the ratios of helicity one and two to helicity

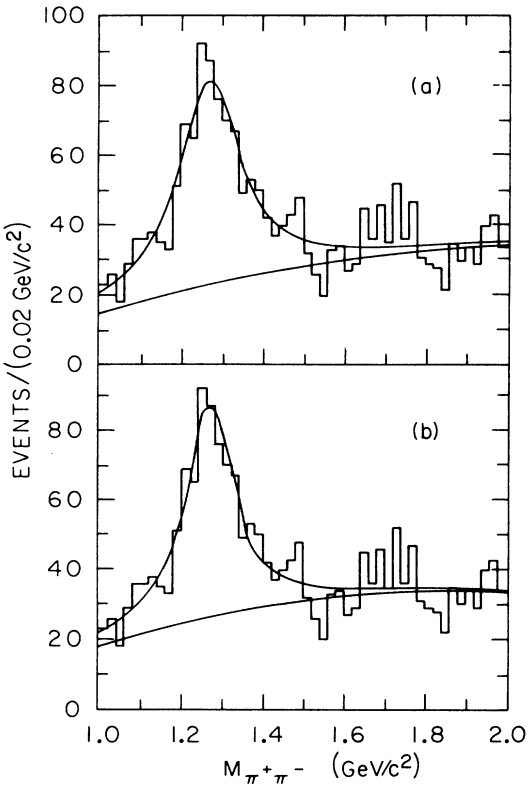

FIG. 7. Fits to the $f(1270)$ (a) with the $f(1270)$ width fixed and (b) with the width allowed to vary.

zero. The fitting procedure involves a maximum-likelihood technique to perform an acceptance corrected fit to determine the four helicity parameters for a given spin hypothesis. For the $f(1270)$ analysis, J is fixed to be 2.

Three angles describe the production and decay process: θ_γ is the polar angle of the radiative photon in the laboratory system; θ_m is the polar angle of the positive meson in the boson center of mass; ϕ_m is the azimuthal angle of the positive meson in the boson center of mass.

For the $\gamma\pi^+\pi^-$ final state, the Monte Carlo acceptances for these angles are shown in Fig. 8. These represent the probability of detecting a track produced with a flat distribution in each of the three angles. The factor which has the greatest impact on the acceptance is the limited solid angle available for well-measured charged tracks. Several comments can be made on the impact of the acceptance for each angle on the subsequent analysis.

θ_γ. This angle suffers from large corrections due to its correlation with the charged-track directions. The effect is not easily visible in uniform phase space decays, but is more apparent when there are stronger track correlations present. The result is that the acceptance is not well defined in the region of large $|\cos\theta_\gamma|$, which is important in distinguishing a uniform distribution from $1+\cos^2\theta_\gamma$.

θ_m. This angle is defined in the boson center-of-mass frame, and is therefore averaged over laboratory directions. The result is that the acceptance corrections are minimal. θ_m provides the most powerful analyzer for the spin of the boson state.

ϕ_m. This angle, while also defined in the center of mass, requires large acceptance corrections, reducing its analyzing power. The angle ϕ_m is Lorentz invariant, as it is defined in a plane normal to the direction of the boost to the boson center of mass. In the laboratory frame, it is the angle between the production plane containing the beams and the radiative photon, and the decay plane, containing the pions and the radiative photon. When these two planes coincide (at $\phi_m=0,\pi$), it is likely that one of the charged tracks will leave the detector at a large value of $|\cos\theta|$. This results in poor acceptance for this angle, rendering it useless for the spin analysis.

The presence of $\rho\pi$ backgrounds further complicates the polarization analysis. Fortunately, the $f(1270)$ lies in a region of low background, between the $\rho^0\pi^0$ and the $\rho^\pm\pi^\mp$ feed-throughs. To correctly account for this back-

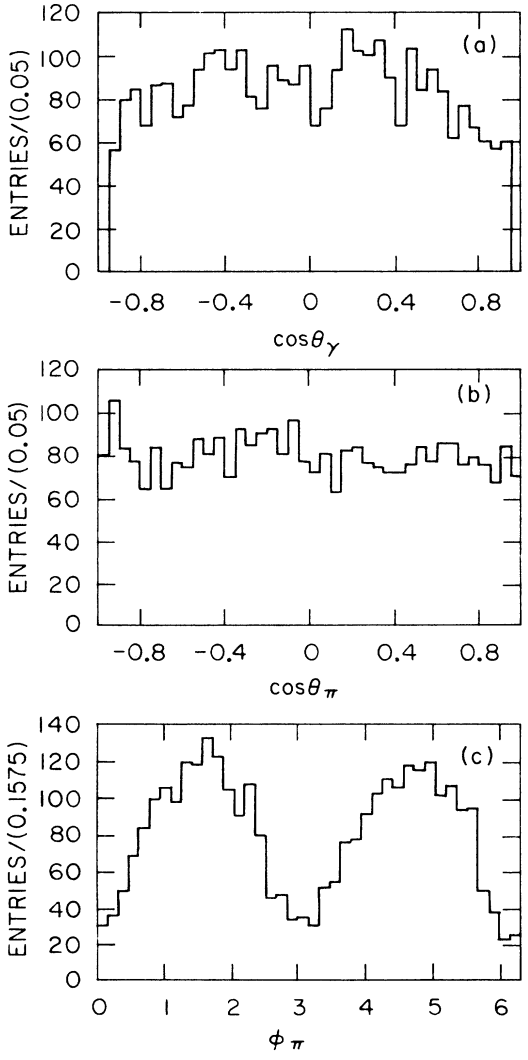

FIG. 8. The Monte Carlo acceptance for the $\gamma\pi^+\pi^-$ final state.

ground in the fitting procedure an additional term is added to the total logarithmic-likelihood function. The, logarithmic-likelihood function for the fit is then

$$\mathcal{L}=(1-\delta)\mathcal{L}_{\gamma\pi\pi}+\delta\mathcal{L}_{\rho\pi} ,$$

where $\mathcal{L}_{\gamma\pi\pi}$ is the $J=2$ angular correlation function, and δ represents the fraction of $\rho\pi$ contamination. The background term, which contains no free parameters, has been calculated using the helicity formalism. The angular correlation function $W_{\rho\pi}$ is

$$W_{\rho\pi}=\sin^2\vartheta_{\pi'}(1+\cos^2\vartheta_{\pi}+\sin^2\vartheta_{\pi}\cos 2\varphi_{\pi'}) ,$$

where ϑ_{π} is the laboratory polar angle of the pion which is not part of the ρ, $\vartheta_{\pi'}$ is the polar angle of the π^+ in the ρ center of mass, and $\varphi_{\pi'}$ is the azimuthal angle of the π^+ in the ρ center of mass. The background logarithmic-likelihood function is

$$\mathcal{L}_{\rho\pi}=[F^{\rho}_{\mathrm{BW}}(\pi\pi)W_{\rho\pi}(\vartheta_{\pi},\vartheta_{\pi'},\varphi_{\pi'})] .$$

The $\pi\pi$ combination which is closest to the ρ mass is used as the ρ. The angles are calculated by using the missing four-momentum recoiling against the $\pi^+\pi^-$ system as an estimate for the missing π^0 four-momentum.

Events to be included in the fit are chosen to lie in a mass region containing the $f(1270)$, $1.15\leq M_{\pi\pi}\leq 1.40$ GeV. The results of applying the likelihood procedure to this event sample are displayed in Fig. 9. The histograms are the data, and the curves are a smoothed approximation to the Monte Carlo prediction for the results of the fit. The fit is a good representation of the data in all three projections displayed here. The results for this fit are

$$x=0.96\pm 0.07,\quad \varphi_x=-0.5\pm 0.7 ,$$

$$y=0.06\pm 0.08,\quad \varphi_y=-0.4\pm 1.9 .$$

The quoted errors are statistical only. The large errors in φ_x and φ_y reflect the minor influence of the relative phases on the fit results. Setting the phases to zero and refitting does not change the values of x and y.

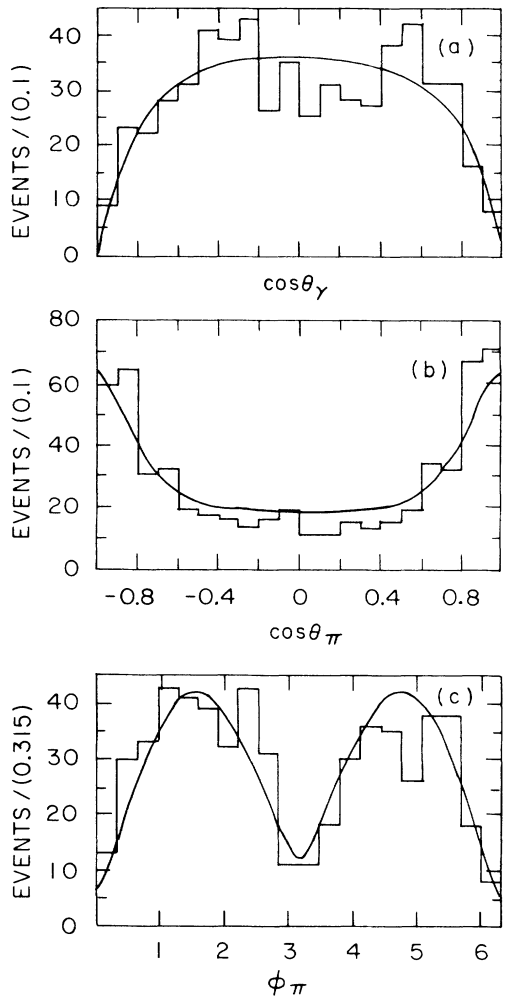

FIG. 9. The histogram is the $f(1270)$ data. The curves are generated by reweighting the Monte Carlo events using the helicity parameters extracted from the maximum-likelihood fit to the data.

Study of radiative decays into other $\pi^+\pi^-$ states

The low-lying 0^{-+} and 2^{++} isoscalar mesons are observed in radiative J/ψ decays with large branching ratios, but there is no evidence for 0^{++} mesons. No limit is set here on the production of the nonstrange state, $\epsilon(1300)$, in radiative J/ψ decays due to the presence of the $f(1270)$. The $S^*(975)$, the 0^{++} isoscalar state with $s\bar{s}$ quark content, lies just below the K^+K^- threshold. It is clearly observed by Mark III in the hadronic decay $J/\psi\rightarrow\phi\pi\pi$ (Ref. 14). It is not observed in $J/\psi\rightarrow\gamma\pi^+\pi^-$, and a limit has been set by performing a maximum-likelihood fit using a Breit-Wigner shape with the mass and width fixed at 0.975 and 0.035 GeV/c^2, respectively:

$$B(J/\psi\rightarrow\gamma S^*)B(S^*(975)\rightarrow\pi\pi)<7\times 10^{-5}$$

(90% C.L.) .

The mass distribution in Fig. 6(a) has two additional structures above the $f(1270)$. The interpretation of these structures is ambiguous, but a fit has been performed to test the hypothesis that the entire spectrum can be described by three incoherent Breit-Wigner functions. The first represents the $f(1270)$ with its mass fixed at 1.270 GeV/c^2 and its width fixed at 0.180 GeV/c^2. The second represents a possible $\theta(1720)$ signal. Its mass has been left free to allow comparison with the K^+K^- results, but its width is fixed at 0.130 GeV/c^2, as seen in the K^+K^- channel. The third Breit-Wigner function represents the third structure observed in the mass distribution. This peak could correspond to an excited $f(1270)$, either the $h(2040)$, with $J^{PC}=4^{++}$, or possibly the corresponding $J^{PC}=2^{++}$ state.

The fit is shown in Fig. 10. The parameters found are

$$m_2=1.713\pm 0.015\ \mathrm{GeV}/c^2 ,$$

$$\Gamma_2\equiv 0.130\ \mathrm{GeV}/c^2\ \text{(fixed)} ,$$

$$m_3=2.086\pm 0.015\ \mathrm{GeV}/c^2 ,$$

$$\Gamma_3=0.210\pm 0.063\ \mathrm{GeV}/c^2 ,$$

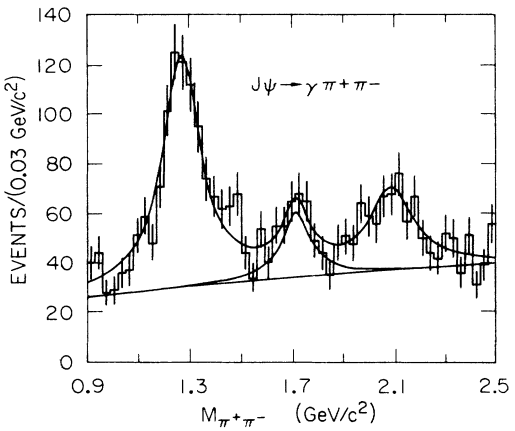

FIG. 10. The $\pi^+\pi^-$ mass distribution with a three-peak fit. The fit represents a possible interpretation for the visible structures and does not include interference effects.

where the errors are statistical only.

The mass obtained in the fit for the second peak is consistent with the $\theta(1720)$ mass of 1.72 GeV measured in the K^+K^- channel. Interpreting this state to be the $\theta(1720)$, and using Monte Carlo events generated with the $\theta(1720)$ parameters found in the K^+K^- system, the efficiency for the cuts applied is 0.39 ± 0.06. This leads to

$$B(J/\psi\to\gamma\theta(1720))B(\theta(1720)\to\pi^+\pi^-) = (1.6\pm0.4\pm0.3)\times10^{-4},$$

where the systematic error includes estimates of the uncertainties in the efficiency due to lack of knowledge of the true angular distributions.

An attempt has been made to study the decay angular distributions of the second peak. Unfortunately, there is significant background, both from the tail of the $f(1270)$ and from $\rho\pi$ event, preventing a full spin analysis. A simpler technique allows the extraction of the angular distribution of the signal events. The θ_π angle contains most of the available information about the spin of the state. To obtain the distribution, the total event sample shown in Fig. 10 is divided into five bins in $|\cos\theta_\pi|$. Fits to the mass distribution corresponding to each such bin are performed to extract the number of observed events in each of the three peaks. The distribution found for the $f(1270)$ is shown in Fig. 11(a). It agrees well with the analysis discussed previously. The distribution for the $\theta(1720)$ and the third peak are shown in Figs. 11(b) and 11(c), and appear flat. As will be shown, this distribution for the $\theta(1720)$ is quite similar to that observed in the K^+K^- channel.

The third peak at $M=2.086$ GeV/c^2 has no obvious interpretation. Its parameters are consistent with those of the $h(2030)$: $m=2.027\pm0.012$ GeV/c^2 and $\Gamma=0.220\pm0.030$ GeV/c^2. Its angular distributions are similar to those of the $\theta(1720)$. Thus, the same efficiency was used to calculate a branching ratio:

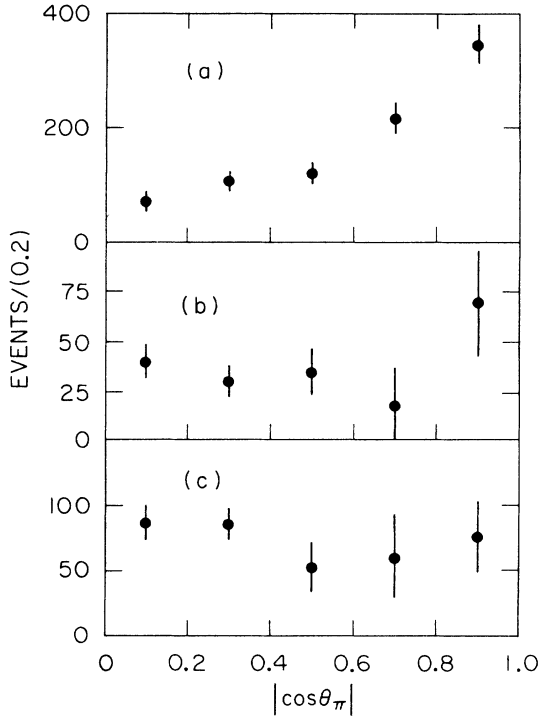

FIG. 11. The extracted $\cos\theta_\pi$ distribution for the peaks: (a) the number of events vs $\cos\theta_\pi$ for the $f(1270)$; (b) for the $\theta(1720)$; (c) for the third peak in the fit.

$$B(J/\psi\to\gamma X(2100))B(X(2100)\to\pi^+\pi^-) = (3.0\pm0.5\pm0.6)\times10^{-4}.$$

One final speculation has been investigated. In previous studies of $J/\psi\to\gamma\pi\pi$ by the Mark II and Crystal Ball Collaborations,[6,5] there was a hint of structure on the high side of the $f(1270)$. This feature is also visible in Fig. 10. The decay $J/\psi\to\omega\pi^+\pi^-$ studied by Mark III has a very large quasi-two-body decay mode: $J/\psi\to\omega f(1270)$, with high statistics.[14] In this final state, there is no indication for structure on the high side of the $f(1270)$.

As possible explanation, a fit is made to four interfering Breit-Wigner amplitudes, including a contribution from $f'(1525)\to\pi^+\pi^-$. This is shown in Fig. 12. The masses and widths of $f(1270)$, $f'(1525)$, and $\theta(1720)$ are fixed:

$$m_f=1.270\ \text{GeV}/c^2,\ \Gamma_f=0.180\ \text{GeV}/c^2,$$
$$m_{f'}=1.520\ \text{GeV}/c^2,\ \Gamma_{f'}=0.080\ \text{GeV}/c^2,$$
$$m_\theta=1.720\ \text{GeV}/c^2,\ \Gamma_\theta=0.130\ \text{GeV}/c^2.$$

The relative magnitudes and phases of each Breit-Wigner amplitude are allowed to vary. The small peak in the $f'(1525)$ region corresponds to the squared amplitude for the $f'(1525)$ from the fit. This corresponds to a product branching ratio of $\sim3\times10^{-5}$. This implies

$$\frac{B(f'\to\pi\pi)}{B(f'\to K\bar{K})}\sim0.05,$$

where the value for the f' product branching ratio to $K\bar{K}$

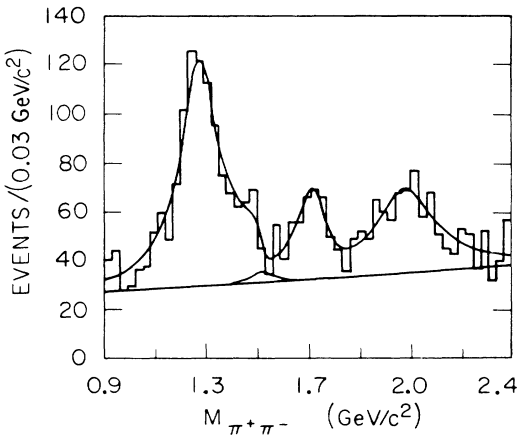

FIG. 12. Fit to $J/\psi \to \gamma\pi^+\pi^-$ containing four interfering Breit-Wigner amplitudes. The additional peak corresponds to a possible signal for the $f'(1525) \to \pi^+\pi^-$.

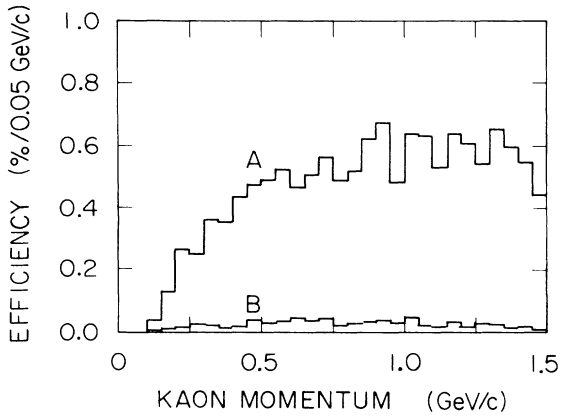

FIG. 13. Single-track kaon efficiency vs momentum: (a) non-decaying kaons, (b) kaons decaying in the drift chamber.

has been taken from the analysis of the K^+K^- channel presented later.

IV. THE γK^+K^- FINAL STATE

Introduction

The $\theta(1720)$ was first observed by the Crystal Ball Collaboration[8] in the $\eta\eta$ mode, using 2.2×10^6 produced J/ψ's. A spin analysis favored $J^P=2^+$ at the 95% C.L. The statistics for this analysis were limited, and no allowance was made for the possible presence of the $f'(1525)$.

The Mark II experiment[8] later observed the $\theta(1720)$ in the K^+K^- mode. Their analysis was able to distinguish the $\theta(1720)$ from the nearby $f'(1525)$ signal.

Kinematics

Since the outer radius of the drift chamber (1.1 m) is comparable to the proper decay length of a kaon (3.7 m), kaons produced in J/ψ decays often decay within the Mark III detector. The detection efficiency for single kaons as a function of momentum is studied using Monte Carlo events. The results are in Fig. 13; the efficiency for detecting kaons falls rapidly below 0.500 GeV/c, and is negligible below 0.200 GeV/c.

The minimum and maximum kaon momenta for different K^+K^- masses are displayed in Fig. 14. The vanishing minimum momentum that occurs at $m_{KK}\sim1.35$ GeV is the result of a kinematic crossover which takes place when the velocity of the K^+K^- system is equal to the velocity of the kaons in the K^+K^- center of mass. This kinematic effect combines with the kaon detection efficiency to produce a reduction in the overall efficiency in the 1.4-GeV/c^2 mass region. This is significant for the $f'(1525)$ branching-ratio measurement and spin analysis.

Event selection

The events are required to have one to four cleanly isolated photons. Charged tracks must be well measured in the drift chamber, and identified as being consistent with kaons by the TOF system. Figure 14 shows that the maximum kaon momentum is always above 1 GeV/c^2. The ability of the TOF system to separate kaons from pions at momenta above 1 GeV/c^2 is very limited. Each track is required to be consistent with the kaon hypothesis within the 2.5σ, corresponding to a weight ≥0.05, where the weight is defined by $e^{-x^2/2}$ with

$$\chi^2=\left[\frac{t_{\text{meas}}-t_{\text{pred}}}{\sigma_t}\right]^2.$$

Although π-K separation of TOF may be ambiguous for a single high-momentum track, the pair identification is satisfactory because the second kaon has low momentum. It is further required that the track is not consistent with the pion hypothesis. This is done by requiring that the relative TOF weight, weight (π)/weight (K), be less than one for each charged track. This cut introduces a slight momentum dependence in the efficiency for kaons with momenta above 1 GeV/c. The overall efficiency for the K^+K^- system is almost independent of the individual

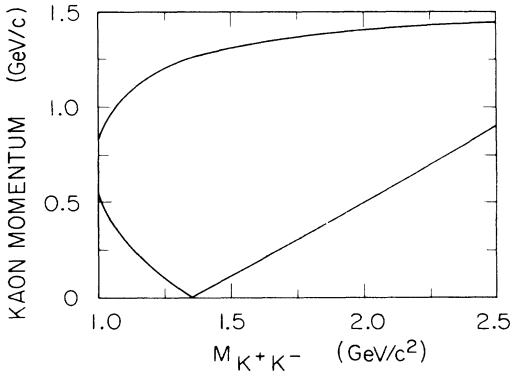

FIG. 14. The minimum and maximum kaon momenta vs $m_{K^+K^-}$.

kaon momenta, except for low $m_{K\bar{K}}$ masses.

Kinematic fits are performed to impose energy and momentum conservation. These fits produce an improvement in the resolution and aid in rejecting background events. Fits to the $J/\psi\to\gamma K^+K^-$ hypothesis are performed using all of the "isolated" photons in the event and the fit with the smallest χ^2 is used. The confidence level for the kinematic fit is required to be greater than 0.02. Monte Carlo studies indicate that less than 5% of these events contain a decay kaon. The distribution of events obtained after making the event selection cuts is shown in Fig. 15.

The background events not eliminated by TOF and kinematic fitting are those containing extra low-energy photons. The dominant contribution comes from the decay $J/\psi\to K^{*\pm}K^{\mp}$, where $K^*\to K\pi^0$. The contribution of these events in the $m_{K\bar{K}}\leq 2.0$ GeV/c^2 region is estimated to be ~ 30 events, or 5% of the total. This background is not rejected.

Mass-plot analysis for the $f'(1525)/\theta(1700)$ region

Two states are apparent in the K^+K^- mass plot shown in Fig. 15. The lower peak is identified with the $f'(1525)$, while the upper peak has a mass consistent with that of the $\theta(1720)$.

To extract the masses and widths for the $f'(1525)$ and the $\theta(1720)$, the mass plot is fitted with two incoherent Breit-Wigner amplitudes, and a parametrization of three-body phase space. The fit is shown in Fig. 15. The parameters obtained are

$$m_{f'}=1.527\pm 0.008 \text{ GeV}/c^2 ,$$

$$\Gamma_{f'}=0.087\pm 0.037 \text{ GeV}/c^2 ,$$

$$m_{\theta}=1.72\pm 0.007 \text{ GeV}/c^2 ,$$

$$\Gamma_{\theta}=0.132\pm 0.015 \text{ GeV}/c^2 .$$

The quoted errors are statistical only. Allowing the two Breit-Wigner amplitudes to interfere does not improve the fit.

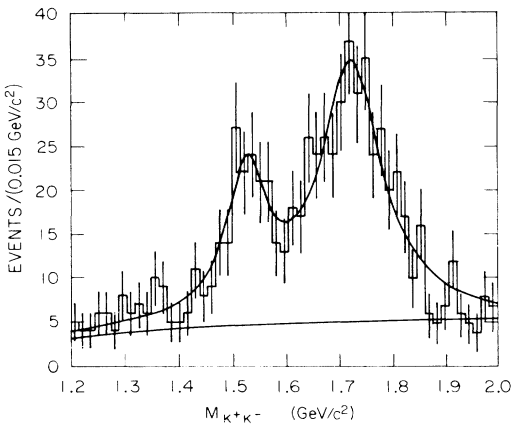

FIG. 15. Incoherent fits to the $f'(1525)$ and the $\theta(1720)$ in the K^+K^- mass distribution.

Spin analysis for the $f'(1525)/\theta(1700)$ region

The next step is to perform a spin analysis using the production and decay angular distributions. The calculation of the production and decay angular distribution for this case has already been described in the discussion of the $f(1270)$. In the present case, the spin will not be assumed; fits will be performed to the $J^P=0^+$ and 2^+ hypotheses.

For the $J=0$ case, the angular distribution is completely determined. For $J=2$, the four parameters, $(x,y,\varphi_x,\varphi_y)$ are *a priori* unknown, and allow the angular distributions to vary greatly in shape. The ability to separate different values of the spin is compromised by this uncertainty. For some values of x and y, states with $J=2$ will have a highly peaked distribution in $\cos\theta_K$, which allows them to be distinguished from $J=0$ states. However, if the $\cos\theta_K$ distribution is approximately flat, it is very difficult to distinguish different spins without high statistics.

The spin analysis is performed separately for the $f'(1525)$ and the $\theta(1720)$ mass regions, defined to be

$$f'(1525):\ 1.45\leq m_{K^+K^-}\leq 1.60 \text{ GeV}/c^2 ,$$

$$\theta(1720):\ 1.60\leq m_{K^+K^-}\leq 1.85 \text{ GeV}/c^2 .$$

Additional cuts were made on the track angles to restrict the fiducial volume

$$|\cos\theta_\gamma|\leq 0.95,\quad |\cos\theta_K|\leq 0.75 .$$

The final event sample contains 103 events in the $f'(1525)$ region and 239 events in the $\theta(1720)$ region. The two resonances are too close in mass to be fully isolated from each other. Using the previous incoherent Breit-Wigner fit as a guide, the $\theta(1720)$ contamination in the $f'(1525)$ region is $\sim 20\%$, and the $f'(1525)$ contamination in the $\theta(1720)$ region is $\sim 5\%$. The influence of this contamination will be studied by performing fits over subintervals of these two regions.

The Monte Carlo acceptances are displayed for the $f'(1525)$ and $\theta(1720)$ regions in Fig. 16. The differences in the acceptance between the $f'(1525)$, and the $\theta(1720)$ are due to kinematic effects and K decays.

The fit procedure is performed under a variety of conditions. The first group of fits is performed over the full $f'(1525)$ region. Two fits to $J=2$ are made: one has the relative phases ϕ_x and ϕ_y fixed at zero; the other allows them to vary. A second group of fits is performed over a restricted mass region, which contains less background from the $\theta(1720)$. The results for this second group are consistent with those from the full mass region, which are displayed in Fig. 17. The curves are a smoothed fit to Monte Carlo events which have been weighted by the actual fit results. This indirect technique is necessary because the acceptance function is never explicitly evaluated, but appears only in the form of a normalization integral. The results for the spin analysis of the $f'(1525)$ region are summarized in Table I. Spin 2 is clearly favored.

It is evident that the acceptance effects are large for this mass region. The $\cos\theta_\gamma$ distribution for $J=0$ before acceptance corrections is $1+\cos^2\theta_\gamma$, whereas after the

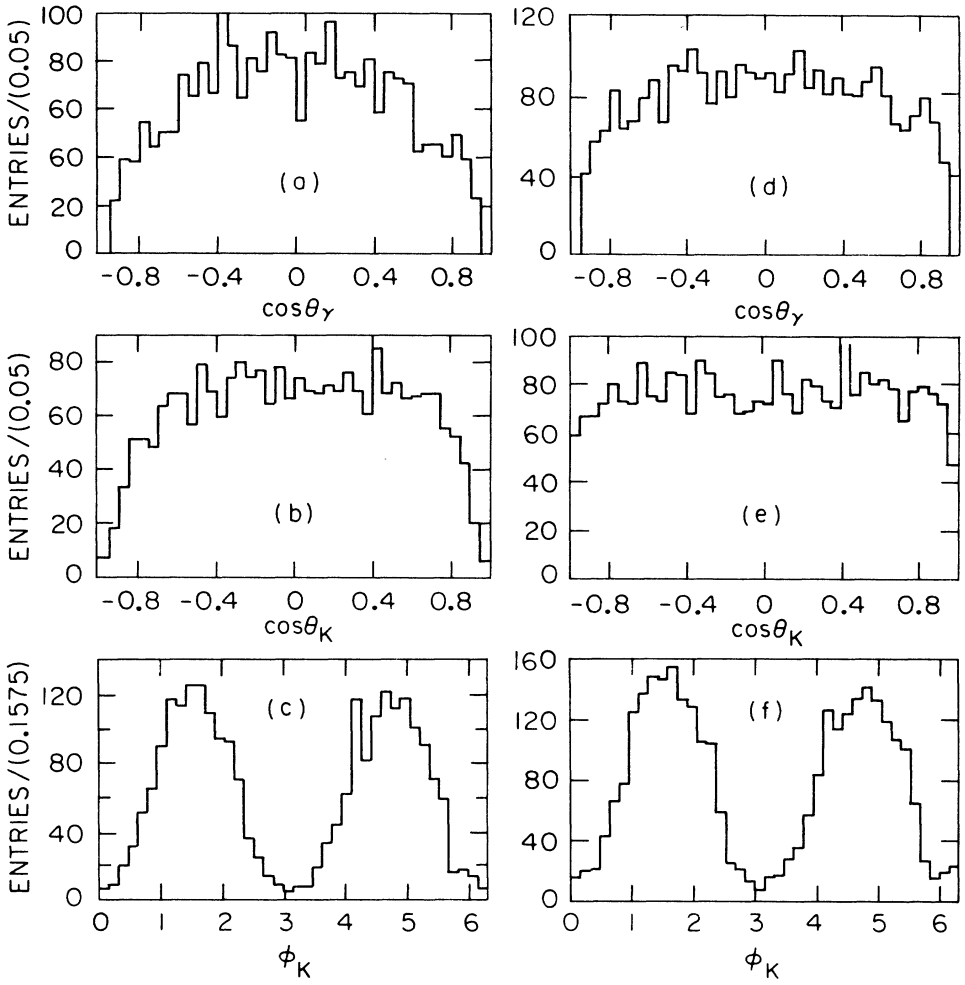

FIG. 16. The acceptances for the $f'(1525)/\theta(1720)$ spin analysis: (a), (b), and (c) are the distributions for the $f'(1525)$ region, (d), (e), and (f) are the distributions for the $\theta(1720)$ region.

corrections it appears approximately flat. The $J=2$ fit appears, in projection, to be slightly better than the $J=0$ fit. Neither fit describes the excess of events near $\cos\theta_K=-1$ very well.

The likelihood is much better for the $J=2$ fit than for the $J=0$ fit. An estimate which takes the number of free parameters into account is obtained by defining

$$\chi^2=-2\ln\left[\frac{\mathscr{L}(J=0)}{\mathscr{L}(J=2)}\right]\sim 43\ .$$

This variable should be distributed like a χ^2 variable for four degrees of freedom, since there are four more variables in the $J=2$ fit than there are in the $J=0$ fit. This would imply that $J=0$ is rejected at the 10^{-6} level.

A better means of evaluating the significance of the fit involves performing a series of Monte Carlo experiments using pure samples consisting of the number of events actually observed. For the $f'(1525)$ region, two sets of Monte Carlo experiments are performed. The first used events generated with $J^P=0^+$, the second, events generated with $J^P=2^+$ and with $x=0.67$, $y=0$, $\varphi_x=\varphi_y=0$. The latter values are chosen as a representative set of parameters from the $J=2$ fit to the real events. The results of a large number of such Monte Carlo experiments, each containing 103 events in the $f'(1525)$ mass region, imply that the relative probability for the $J^P=0^+$ hypothesis is $\leq 10^{-3}$.

The conclusion of this analysis is that the $f'(1525)$ has $J^P=2^+$, which agrees with the established value.[12] The helicity-amplitude ratios measured here for the first time are $x\sim\frac{2}{3}$ and $y\sim 0$. The corresponding phases are consistent with zero. These values agree qualitatively with those found for the $f(1270)$ presented earlier in this paper.

The analysis of the $\theta(1720)$ region proceeds in an identical manner. The results of the spin analysis are summarized in Table II. The results for fits to the full $\theta(1720)$ region are listed, along with the results for fits performed in a subinterval with less potential $f'(1525)$ contamination. The results for the two groups of fits are consistent. Once again, the three projections indicate that $J=2$ yields a better description of the data. The likelihood ratios in-

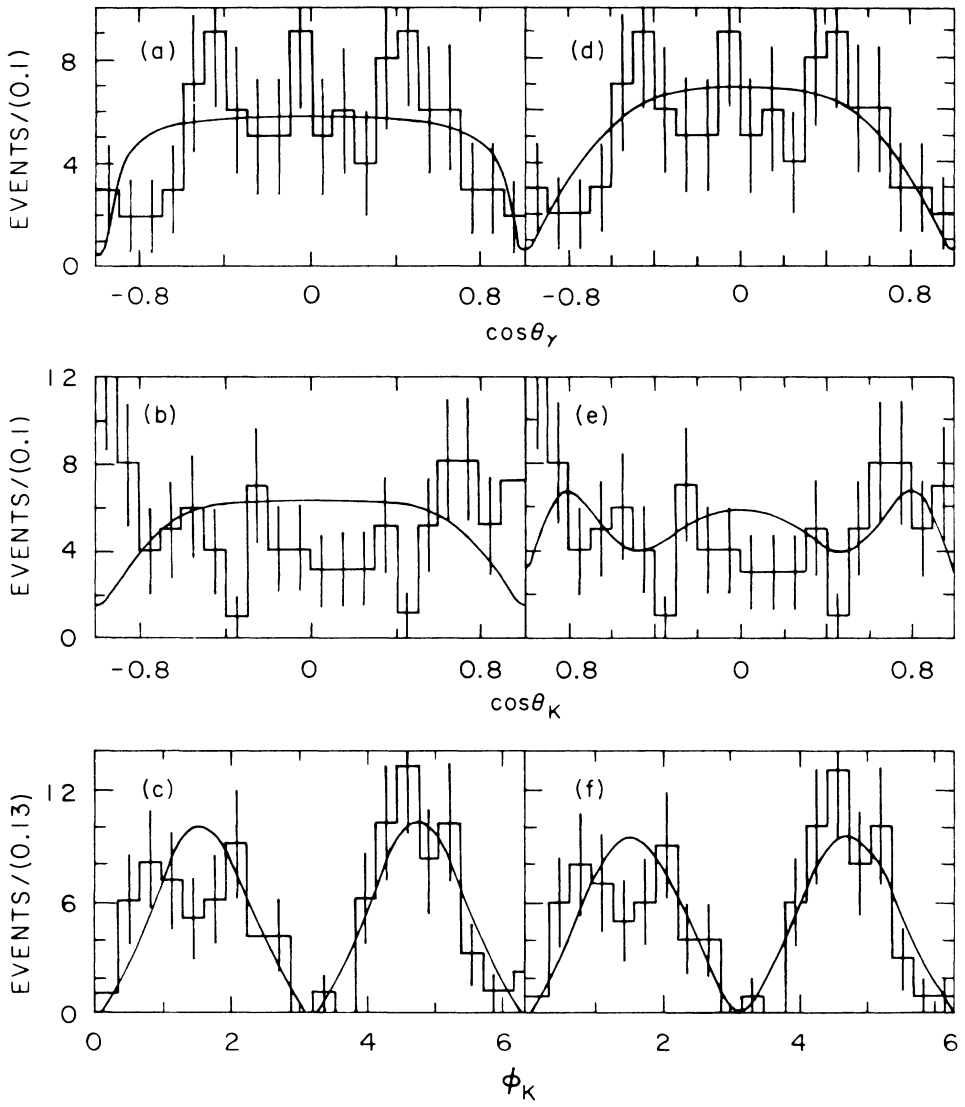

FIG. 17. The fit results for the $f'(1525)$ spin analysis. The histograms display the events used in the fit. (a), (b), and (c) indicate the results for the $J=0$ fit, (d), (e), and (f) for the $J=2$ fit. (See Fig. 9 for details.)

TABLE I. The $f'(1525)$ spin-analysis results. The upper group of fits are performed over the full mass region. The lower group of fits has fewer events, but has less $\theta(1720)$ contamination.

Full $f'(1525)$ region	Fit $J=0$	$\ln\mathscr{L}=-257.5$
	Fit $J=2$	$\ln\mathscr{L}=-237.3$
$1.45\leq m\leq 1.60$ GeV/c^2	(fixed phases)	$x=0.65\pm0.09$, $\varphi_x=0$
103 events		$y=-0.03\pm0.11$, $\varphi_y=0$
	Fit $J=2$	$\ln\mathscr{L}=-235.9$
	(variable phases)	$x=0.63\pm0.09$, $\varphi_x=1.3\pm0.6$
		$y=0.17\pm0.15$, $\varphi_y=2.6\pm0.9$
Partial $f'(1525)$ region	Fit $J=0$	$\ln\mathscr{L}=-84.2$
	Fit $J=2$	$\ln\mathscr{L}=-81.6$
$1.450\leq m\leq 1.525$ GeV/c^2	(variable phases)	$x=0.85\pm0.23$, $\varphi_x=1.1\pm0.8$
43 events		$y=-0.4\pm0.3$, $\varphi_y=1.3\pm1.0$

TABLE II. The $\theta(1720)$ spin-analysis results. The upper group of fits are performed over the full mass region. The lower group of fits are performed over a restricted mass region.

Full $\theta(1720)$ region	Fit $J=0$	$\ln\mathscr{L}=-644.9$
	Fit $J=2$	$\ln\mathscr{L}=-636.7$
$1.60\leq m\leq 1.85$ GeV/c^2	(fixed phases)	$x=-1.07\pm0.16$, $\varphi_x=0$
239 events		$y=-1.10\pm0.16$, $\varphi_y=0$
	Fit $J=2$	$\ln\mathscr{L}=-636.5$
	(variable phases)	$x=-1.07\pm0.16$, $\varphi_x=0.6\pm0.6$
		$y=-1.09\pm0.15$, $\varphi_y=-0.1\pm0.5$
Partial $\theta(1720)$ region	Fit $J=0$	$\ln\mathscr{L}=-438.8$
	Fit $J=2$	$\ln\mathscr{L}=-432.9$
$1.675\leq m\leq 1.850$ GeV/c^2	(variable phases)	$x=-1.14\pm0.20$, $\varphi_x=0.0\pm1.1$
177 events		$y=-1.28\pm0.20$, $\varphi_y=0.0\pm0.9$

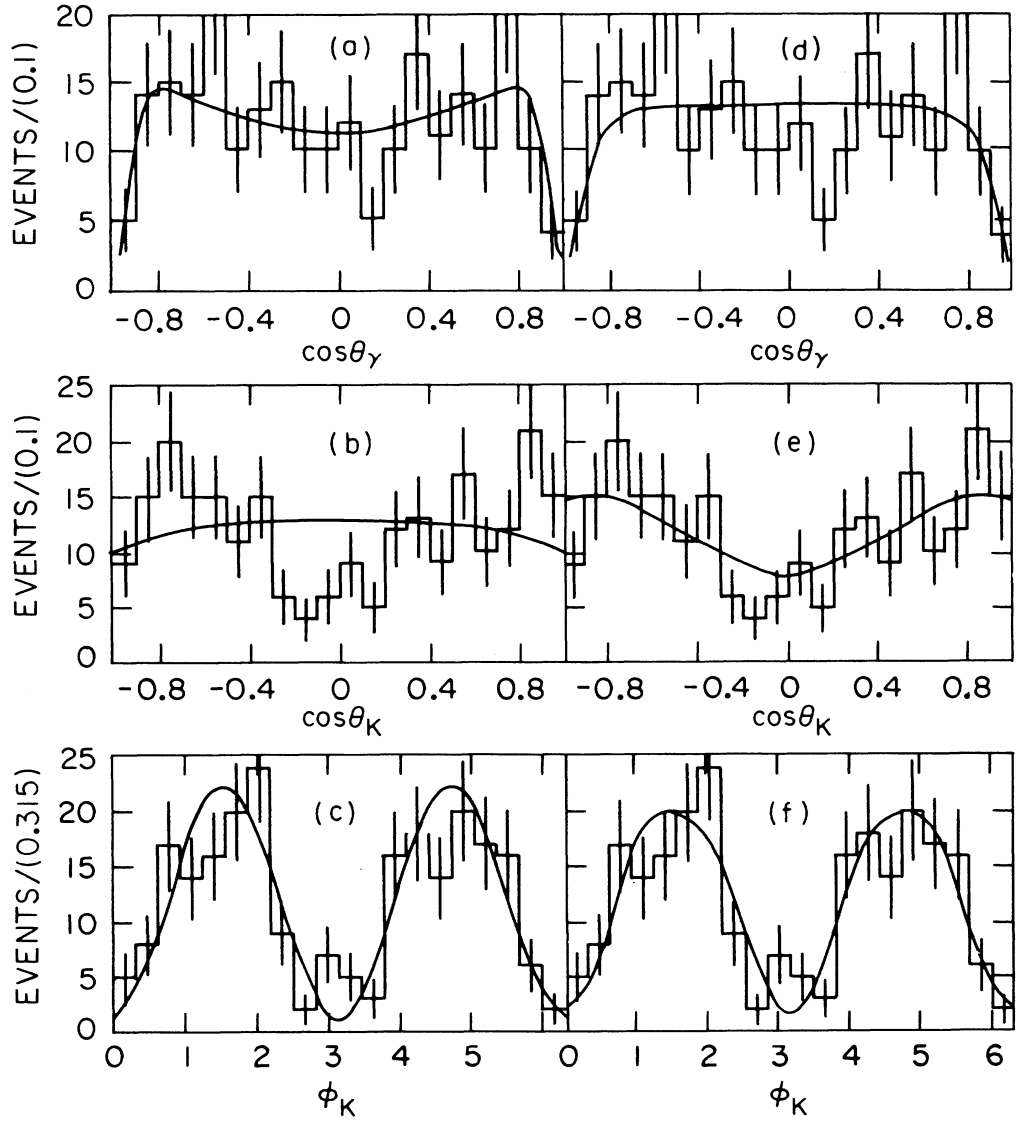

FIG. 18. The fit results for the $\theta(1720)$ spin analysis. The histograms display the events used in the fit. (a), (b), and (c) indicate the fit results for the $J=0$ fit, (d), (e), and (f) for the $J=2$ fit. (See Fig. 9 for details.)

dicate the same trend, but not as strongly as for the $f'(1525)$ fits. The corresponding estimate for the significance of these results gives

$$\chi^2=-2\ln\left[\frac{\mathscr{L}(J=0)}{\mathscr{L}(J=2)}\right]\sim 17 .$$

Assuming a χ^2 distribution for four degrees of freedom gives a confidence level of about 2×10^{-3}, strongly favoring the $J^P=2^+$ hypothesis for the $\theta(1720)$.

The most important feature of the projections is the nonflat distribution in $\cos\theta_K$ (Fig. 18). It is described fairly well by the $J=2$ fit, but very poorly by the $J=0$ fit.

For the $\theta(1720)$ region, two ensembles of Monte Carlo experiments are also performed. The first uses events generated with $J^P=0^+$, and the second, events generated with $J^P=2^+$, and with $x=-1.2$, $y=-1.2$, $\varphi_x=\varphi_y=0$. The values measured for x and y in the real data do not agree with the values expected from the Monte Carlo tests if the $\theta(1720)$ were really a $J^P=0^+$ state. Monte Carlo experiments generated with $J=2$ agree quite well with the measured values, and indicate that $\theta(1720)$ is very consistent with the $J^P=2^+$ parent distribution.

The conclusion of this analysis is that the $\theta(1720)$ is a $J^P=2^+$ state. The Monte Carlo experiments, although indicating that the $J=2$ likelihood should be larger, suggest a relative probability for $J=0$ of $\sim10^{-3}$.

Branching ratios for the $f'(1525)/\theta(1700)$ region

To calculate a branching ratio, the $f'(1525)$ efficiency is measured by using Monte Carlo events generated with the following parameters:

$$m=1.520\ \text{GeV}/c^2,\quad \Gamma=0.075\ \text{GeV}/c^2 ,$$
$$J=2,\quad x=0.67,\quad y=0.0,\quad \varphi_x=\varphi_y=0 .$$

After passing these events through the standard event selection procedure the resulting detection efficiency is

$$\epsilon_{f'}=0.160\pm0.024 .$$

A similar procedure is used for the $\theta(1720)$ detection efficiency. The Monte Carlo events are generated with the following parameters:

$$m=1.725\ \text{GeV}/c^2,\quad \Gamma=0.120\ \text{GeV}/c^2 ,$$
$$J=2,\quad x=-1.2,\quad y=-1.2,\quad \varphi_x=\varphi_y=0 .$$

The detection efficiency is

$$\epsilon_\theta=0.222\pm0.033 .$$

The large difference between the $f'(1525)$ and the $\theta(1720)$ detection efficiencies is due to the acceptance effects discussed previously.

These efficiencies, when combined with the number of J/ψ's which were produced and the number of observed events, yield the following branching ratios:

$$B(J/\psi\to\gamma f'(1525))B(f'(1525)\to K^+K^-)=(3.0\pm0.7\pm0.6)\times10^{-4} ,$$
$$B(\psi\to\gamma\theta(1720))B(\theta(1720)\to K^+K^-)=(4.8\pm0.6\pm0.9)\times10^{-4} .$$

V. THEORETICAL DISCUSSION

The $f(1270)$ and $f'(1525)$ are the two isosinglet members of the lowest-lying $q\bar{q}$ tensor nonet. This nonet is experimentally observed to be almost ideally mixed; the $f(1270)$ is nearly pure $u\bar{u}+d\bar{d}$ and the $f'(1525)$ nearly pure $s\bar{s}$. For the standard J/ψ radiative decay diagram, the photon is radiated from the initial state, and the two-gluon system is an SU(3) singlet. This predicts[15] the ratio

$$R=\frac{\Gamma(J/\psi\to\gamma f')}{\Gamma(J/\psi\to\gamma f)}=0.5$$

if phase-space corrections are ignored. R cannot be evaluated exactly because $B(f'(1525)\to K\bar{K})$ is not known. Using the Mark III values for the radiative ratios to $\pi\pi$ and KK presented here earlier and the value $B(f(1270)\to\pi\pi)=0.83\pm0.02$ (Ref. 12), one obtains

$$R=\frac{0.43\pm0.15}{B(f'(1525)\to K\bar{K})} .$$

Montanet[16] has quoted a lower bound: $B(f'\to K\bar{K})\geq0.7$. If a value of 0.8 is assumed, then

$$R=0.54\pm0.19 ,$$

in satisfactory agreement with the SU(3)-singlet prediction.

For the $\theta(1720)$, the values of x and y give information about its internal dynamical structure. Krammer,[17] using $E1$ dominance, predicts $x=\sqrt{3}$, $y=\sqrt{6}$. This is the correct answer for the radiative production and decay of $\chi(3555)$, from the ψ' resonance. Bugg[18] showed that if the $\theta(1720)$ is a light quark-antiquark state with $l=1$, then one expects the relation $2\sqrt{2}x-\sqrt{6}=y$. This relation is satisfied by Krammer's values, but not by the present measurements of $x\approx-1$, $y\approx-1$. Close[19] has argued that, if the transverse momentum in a light $q\bar{q}$ spin-2 state with mass equal to m_θ is small with respect to $(m_{J/\psi}^2-m_\theta^2)/2m_{J/\psi}$, one expects $x\approx\sqrt{3/2}$, $y\approx0$, in contradiction with our data for the $\theta(1720)$, but correct for the $f(1270)$ and the $f'(1525)$. Close's values also satisfy Bugg's relation. Liu[20] pointed out that the x and y values from a $qq\bar{q}\,\bar{q}$ interpretation of the $\theta(1720)$ are inconsistent with this data. Ward,[21] presuming the $\theta(1720)$ to be a bound state of two transverse-electric gluons, and using Lipkin's idea of $\chi_2(3555)$ dominance[22] in an effective-Lagrangian formalism, found $x\approx-0.85$, $y\approx-1.0$, with theoretical uncertainties of 25%. These results support the popular view that the $\theta(1720)$ is a $(\text{TE})^2$ glueball state, but that a $q\bar{q}G$ state is not excluded.

VI. EXPERIMENTAL SUMMARY

In the $\gamma\pi^+\pi^-$ final state, the $f(1270)$ is observed with a mass and width that agree well with the standard values.

Because of the correlation between the width and the background shape, a fixed $f(1270)$ width has been used. The quoted branching ratio comes from a fit using three incoherent Breit-Wigner line shapes to describe the $\pi^+\pi^-$ mass spectrum. The result is

$$B(J/\psi\to\gamma f(1270))B(f(1270)\to\pi\pi) = (1.15\pm0.07\pm0.19)\times10^{-3} .$$

This is in good agreement with the best previous measurements.[6]

A polarization analysis of the $f(1270)$ has been performed. The results shown below include estimated systematic effects in the fitting procedure, mostly associated with the large $\rho\pi$ background. These results are

$$x = 0.96\pm0.12, \quad \varphi_x = -0.5\pm0.7 ,$$
$$y = 0.06\pm0.13, \quad \varphi_y = -0.4\pm1.9 .$$

The best previous measurement[6] yielded

$$x = 0.88\pm0.11, \quad y = 0.04\pm0.14 .$$

A limit has been set on the radiative production of the scalar state $S^*(975)$:

$$B(J/\psi\to\gamma S^*(975))B(S^*(975)\to\pi\pi) < 7\times10^{-5} \quad (90\%\ \text{C.L.}) .$$

In $J/\psi\to\gamma\pi^+\pi^-$ there is evidence for additional structure at high $\pi^+\pi^-$ masses. This can be interpreted in terms of production of the $\theta(1720)$ and an additional broad resonance with a mass of ~2.1 GeV/c^2. The observed mass, width, and $\cos\theta_\pi$ distributions for the $\theta(1720)$ are consistent with those observed in the K^+K^- channel. No clear interpretation exists for the higher-mass resonance at 2.1 GeV/c^2. The branching ratio has been obtained for $\theta(1720)$ by assuming the decay-angular distributions are the same as those found in the K^+K^- channel:

$$B(J/\psi\to\gamma\theta(1720))B(\theta(1720)\to\pi^+\pi^-) = (1.6\pm0.4\pm0.3)\times10^{-4} .$$

These values are consistent with the previous measurement of this final state.[5] The higher-mass peak $X(2100)$ has the following properties:

$$m = 2.086\pm0.015\ \text{GeV}/c^2 ,$$
$$\Gamma = 0.210\pm0.063\ \text{GeV}/c^2 ,$$
$$B(J/\psi\to\gamma X(2100))B(X(2100)\to\pi^+\pi^-) = (3.0\pm0.5\pm0.6)\times10^{-4} .$$

In the γK^+K^- final state, the $f'(1525)$ and the $\theta(1720)$ have been observed. The masses and widths have been measured:

$$m_{f'} = 1.525\pm0.010\pm0.010\ \text{GeV}/c^2 ,$$
$$\Gamma_{f'} = 0.085\pm0.035\ \text{GeV}/c^2 ,$$
$$m_\theta = 1.720\pm0.010\pm0.010\ \text{GeV}/c^2 ,$$
$$\Gamma_\theta = 0.130\pm0.020\ \text{GeV}/c^2 .$$

These agree well with the standard values.[12]

The spins and the helicity-amplitude ratios for the $f'(1525)$ and $\theta(1720)$ have been measured. The relative phases have been found to be consistent with zero, and

$$J^P(f') = 2^+ \text{ at } \sim99.9\%\ \text{C.L.} ,$$
$$x = 0.63\pm0.10 ,$$
$$y = 0.17\pm0.20 ,$$
$$J^P(\theta) = 2^+ \text{ at } 99.9\%\ \text{C.L.} ,$$
$$x = -1.07\pm0.20 ,$$
$$y = -1.09\pm0.25 .$$

The branching ratios have been measured:

$$B(J/\psi\to f'(1525))B(f'(1525)\to K^+K^-) = (3.0\pm0.7\pm0.6)\times10^{-4} ,$$
$$B(J/\psi\to\theta(1720))B(\theta(1720)\to K^+K^-) = (4.8\pm0.6\pm0.9)\times10^{-4} .$$

The value for the $f'(1525)$ branching ratio presented here is somewhat larger than the previous measurement of $(0.9\pm0.3\pm0.5)\times10^{-4}$ (Ref. 7), while that for the $\theta(1720)$ is consistent.

ACKNOWLEDGMENT

This work was supported in part by the Department of Energy, under Contracts Nos. DE-AC03-76SF00515, DE-AC02-76ER01195, DE-AC03-81ER40050, DE-AM03-76SF0034, and by the National Science Foundation.

[1] K. F. Einsweiler, thesis, SLAC Report No. 272, 1984.
[2] R. M. Baltrusaitis *et al.*, Phys. Rev. Lett. **56**, 107 (1986).
[3] S. J. Brodsky, T. A. DeGrand, R. R. Horgan, and D. G. Coyne, Phys. Lett. **73B**, 203 (1978); K. Koller and T. Walsh, Nucl. Phys. **B140**, 449 (1978).
[4] A. Billoire *et al.*, Phys. Lett. **80B**, 381 (1979); R. Lacaze and H. Navelet, Nucl. Phys. **B186**, 247 (1981).
[5] D. L. Scharre, in *Lepton and Photon Interactions at High Ener-*

gies, proceedings of the International Symposium, Bonn, 1981, edited by W. Pfeil (Bonn University, Physics Institute, Bonn, 1981).
[6]C. Edwards *et al.*, Phys. Rev. D **25**, 3065 (1982).
[7]C. Edwards *et al.*, Phys. Rev. Lett. **48**, 458 (1982).
[8]M. E. B. Franklin, thesis, SLAC Report No. 254, 1982.
[9]D. L. Scharre, in *Field Theory and Elementary Particles,* proceedings of Orbis Scientiae, Coral Gables, 1982, edited by A. Perlmutter (Plenum, New York, 1982).
[10]D. Bernstein *et al.*, Nucl. Instrum. Methods **226**, 301 (1984).
[11]T. Himel *et al.*, Phys. Rev. Lett. **45**, 1146 (1980).
[12]Particle Data Group, Rev. Mod. Phys. **56**, S1 (1984).
[13]M. Jacob and G. C. Wick, Ann. Phys. (N.Y.) **7**, 404 (1959); J. D. Richman, Caltech Report No. CALT-68-1148, 1984 (unpublished).
[14]U. Mallik, in *Strong Interactions and Gauge Theories,* proceedings of the 21st Recontre de Moriond, 1986, edited by J. Tran Thanh Van (Editions Frontieres, Gif-sur-Yvette, 1986).
[15]H. J. Lipkin and H. R. Rubenstein, Phys. Lett. **76B**, 342 (1978).
[16]L. Montanet, Rep. Prog. Phys. **46**, 337 (1983).
[17]M. Krammer, Phys. Lett. **74B**, 361 (1978).
[18]D. V. Bugg, CERN report, 1985 (unpublished).
[19]F. E. Close, Phys. Rev. D **27**, 311 (1983).
[20]K. F. Liu, in *Hadron Spectroscopy—1985,* proceedings of the International Conference, College Park, Maryland, edited by S. Oneda (AIP Conf. Proc. No. 132) (AIP, NY, 1985), p. 90.
[21]B. Ward, Phys. Rev. D **33**, 1900 (1986).
[22]H. J. Lipkin (private communication).